



TECHNICAL ARTICLE

Microstructure–Mechanical Property Relationship and Austenite Stability in Transformation-Induced Plasticity Steels: Effects of Quenching and Partitioning Processing and Quenching and Tempering Treatments

Huixin Zuo, Jinfeng Feng, Ying Sun, Qiannan Li, Zhichao Li, Devesh Misra, Lianfang He, and Huiping Li

Submitted: 27 December 2022 / Revised: 6 April 2023 / Accepted: 9 April 2023 / Published online: 17 May 2023

We elucidate here the underlying reason for the differences in mechanical properties of cold-rolled light-weight medium manganese TRIP steel subjected to two unique heat treatments with the objective to optimize the mechanical properties. Furthermore, the relationship between the mechanical properties of the material and the stability of austenite was explored. After quenching and tempering (Q and T) treatment, tensile strength and total elongation of the experimental steel were 942 ± 11 – 1380 ± 22 MPa and 12.5 ± 1.5 – $52.5 \pm 2.1\%$, respectively. While, the tensile strength and total elongation of experimental steel after quenching and partitioning (Q and P) treatment were in the range of 890 ± 10 – 1470 ± 24 MPa and 5 ± 0.8 – $47.4 \pm 1.7\%$, respectively. The primary reason for the difference in mechanical properties is that the volume fraction of austenite in Q and T steel was higher, and the degree of TRIP effect was significantly greater. Interestingly, when the volume fraction of austenite was similar, the elongation of steel after Q and P treatment was greater. Short-time heat treatment results in non-uniform distribution of Mn in austenite grain. The Mn content at the austenite grain boundary regions is higher than that inside the grain, which leads to low stability of austenite. Austenite transforms in the short time during deformation, which cannot provide strong TRIP effect, resulting in low elongation. However, the diffusion time of Mn in the steel heat treated by Q and P is relatively long, the diffusion distribution of Mn in austenite is more uniform, and the stability of austenite is enhanced, which can delay the emergence of TRIP effect during deformation, and provides strong work hardening ability and increases elongation.

Keywords austenite stability, deformation behavior, micro structure evolution, superior mechanical properties, TRIP steel, work hardening

1. Introduction

Medium-Mn transformation-induced plasticity (TRIP) steels are potential steels for lightweight automobile steel of the future because they have excellent mechanical properties (high strength and excellent plasticity). Their excellent combination of high strength and total elongation is mainly attributed to the

TRIP effect during tensile deformation (Ref 1, 2). Generally, the heat treatment of medium-Mn steel, such as austenite-reverted transformation (ART) annealing, takes a long time, which is difficult to achieve in the present steel (Ref 3–5).

Speer (Ref 6) put forward the concept of quenching and partitioning (Q and P) heat treatment and established the model of carbon distribution endpoint between quenched martensite and retained austenite. Subsequently, many studies were carried out on Q and P and medium-Mn TRIP steel. In a study by Lee (Ref 1), the PSE (product of strength and elongation) of 0.05C–6Mn cold-rolled steel was ~ 23 GPa%, while that of 0.1C–6Mn cold-rolled steel was a ~ 30 – 36 GPa% (Ref 7–9). In a study by Pan (Ref 10), Q and P and warm stamping were combined, the PSE was more than 23 GPa%, and the yield strength of medium-Mn steel was significantly improved, which is in line with one of the future development goals of medium-Mn steel, namely, achieving ultra-high tensile strength without reducing ductility (Ref 11, 12).

However, little attention has been paid to the necessity of partitioning steps in Q and P heat treatment and the effect of carbon and manganese distribution between ferrite–austenite and martensite–austenite on the stability of austenite. In this regard, to acquire a detailed understanding, we used Q and P heat treatment process for 0.2C–8.5Mn–3Al–Fe cold-rolled experimental steel and proposed a novel heat treatment process, namely, quenching and tempering at low temperature (Q and T). Subsequently, we compared the tensile strength and

Huixin Zuo, Jinfeng Feng, Ying Sun, Qiannan Li, Lianfang He, and Huiping Li, School of Materials Science and Engineering, Shandong University of Science and Technology, Qingdao 266590 Shandong, China; **Zhichao Li**, School of Materials Science and Engineering, Shandong University of Science and Technology, Qingdao 266590 Shandong, China; School of Materials Science and Engineering, Xiangtan University, Xiangtan 411105 Hunan, China; and Mengshan Steel Structure Engineering Co., Ltd, Jining 272400 Shandong, China; and **Devesh Misra**, Laboratory for Excellence in Advanced Steel Research, Department of Metallurgical, Materials and Biomedical Engineering, University of Texas at El Paso, El Paso, TX 79968. Contact e-mails: lizhichao198918@163.com and lihuiping99@163.com.

elongation of 0.2C-8.5Mn-3Al-Fe cold-rolled steels under Q and P and Q and T processes, and analyzed the microstructure of the steels (Ref 13). The effect of Q and P and Q and T processes on the volume fraction of austenite in the cold-rolled steel and the relationship of C and Mn on the stability of austenite is discussed. The relationship between deformation mechanism of 0.2C-8.5Mn-3Al-Fe cold-rolled steels and mechanical properties is also explored.

2. Materials and Experimental Procedure

The chemical composition of the steel was Fe-0.2C-8.5Mn-3Al (wt.%) with approximately 0.001-0.002 S, P, and Zn measured by atomic absorption spectrometry. The density of steel calculated using atomic percentages is 7.43 g/cm^3 and measured according to Archimedeian principle is 7.24 g/cm^3 . About 40-kg cast ingots were refined utilizing a vacuum melting furnace and then forged into a slab with a cross-sectional dimensions of segment size $30 \text{ mm} \times 100 \text{ mm}$. Then, the forged rods were hot rolled to $\sim 4.0 \text{ mm}$ in thickness with 7 passes after reheating to $1200 \text{ }^\circ\text{C}$ for 2 h, the initial and final rolling temperatures were 1150 and $850 \text{ }^\circ\text{C}$, respectively. The ingots were air cooled to room temperature after hot rolling. Finally, the sheet was cold rolled to 1-mm thick. The rolling process is shown in Fig. 1.

For medium-Mn steel, the traditional ART process requires a long time of intercritical annealing. In order to improve the heat treatment efficiency of the present steel, two novel and efficient heat treatment processes, Q and T and Q and P, were adopted. The heat treatment scheme of Q and T is as follows: (1) In the first process, the cold-rolled experimental steel was heated in the temperature range of A_{c1} - A_{c3} for 5 min and then cooled in water. (2) In the second process, tempering was carried out at $200 \text{ }^\circ\text{C}$ for 2 min. Q and T heat treatment process curve is presented in Fig. 4. In view of smaller morphology of cold-rolled experimental steel, less residual stress and lower grain boundary brittleness are induced by shorter austenitizing holding time (Ref 14), the quenching and tempering heat treatment process was simplified, and no tempering was carried out. The heat treatment scheme of Q and P is as follows: (1) In the first process, quenching, the cold-rolled experimental steel

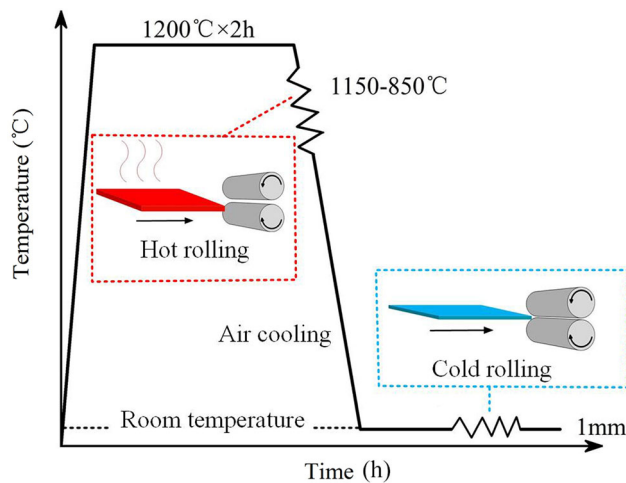


Fig. 1 Rolling process of experimental steel

was heated into the temperature range of A_{c1} - A_{c3} for 5 min and then cooled in the air. (2) In the second process, soaking, after austenitizing, the cold-rolled experimental steel was cooled directly in the temperature range of M_f - M_s and then kept at a temperature for 2 min. (3) In the third process, partitioning, the cold-rolled steel was heated from soaking temperature to partitioning temperature and kept for 5 min, then air cooled to room temperature. Q and P heat treatment process curve is presented in Fig. 3.

Using WDW-200E microcomputer controlled universal testing machine, the tensile test of specimens was carried out at a constant speed of 3 mm min^{-1} . The microstructure was characterized by optical microscope (OM), field emission scanning electron microscopy (SEM, FE-SEM, SSX-550, Supra, Shimadzu, Tokyo, Japan) (the etching agent is 6% nitric alcohol), electron probe microanalysis (EPMA), field emission transmission electron microscopy (TEM, FE-TEM, TECNAI G2-20, FEI, operated at 200 kV , Hillsboro, USA), and x-ray diffraction (XRD, D/Max2250/ PC, Rigaku, Tokyo, Japan).

The volume fraction of austenite under CuK_α radiation was determined by direct comparison method and x-ray diffraction method (Ref 15, 16). The volume fraction of austenite was measured using the integrated intensities of $(220)_\gamma$ and $(311)_\gamma$ peaks of austenite and $(200)_\alpha$ and $(211)_\alpha$ peaks of ferrite. Using Eq. 1 to calculate the volume fraction of austenite V_A (Ref 17, 18):

$$V_A = \frac{\frac{1}{N} \sum_{i=1}^N \frac{I_{\gamma,i}}{R_{\gamma,i}}}{\frac{1}{N} \sum_{i=1}^N \frac{I_{\gamma,i}}{R_{\gamma,i}} + \frac{1}{M} \sum_{i=1}^M \frac{I_{\alpha,i}}{R_{\alpha,i}}} \quad (\text{Eq 1})$$

where I_α and I_γ are integrated intensity values of ferrite α -phase and austenite, respectively. M and N are the numbers of ferrite peaks and austenite peaks, respectively. R_α and R_γ are the standardization constant of ferrite and austenite, respectively. $R_{\gamma, (220)} = 1.796 \text{ m}^{-1}$, $R_{\gamma, (311)} = 2.282 \text{ m}^{-1}$, $R_{\alpha, (211)} = 2.932 \text{ m}^{-1}$, and $R_{\alpha, (200)} = 1.269 \text{ m}^{-1}$.

In order to ensure a proper heat treatment schedule, the intercritical region was obtained by thermal expansion method. The sample used for thermal expansion measurement is a solid cylindrical sample with a length of 10 mm and a diameter of 3 mm . The dilatometric curve of the experimental steel is presented in Fig. 2. After thermal expansion in the heating stage (20 - $1000 \text{ }^\circ\text{C}$) at the rate of $20 \text{ }^\circ\text{C/s}$, the sample was held at $1000 \text{ }^\circ\text{C}$ for 3 min. It is clear that no transformation took place in the sample during the fast cooling, at the rate of $100 \text{ }^\circ\text{C s}^{-1}$, until martensite start (M_s) temperature. As marked in Fig. 2, the intercritical temperature range of the steel is 629 - $867 \text{ }^\circ\text{C}$, and the M_s temperature is $180 \text{ }^\circ\text{C}$.

The Q and P samples were intercritically annealed in the temperature range of 650 - $850 \text{ }^\circ\text{C}$ at $50 \text{ }^\circ\text{C}$ intervals for 5 min. The soaking temperature should be between M_s and M_f , so the samples were soaked at $100 \text{ }^\circ\text{C}$, and the partition temperature was $350 \text{ }^\circ\text{C}$, and the heat treatment process is shown in Fig. 3. The intercritical annealing temperatures of Q and T samples were in the range of 600 - $800 \text{ }^\circ\text{C}$ at $50 \text{ }^\circ\text{C}$ intervals. The heat treatment process is shown in Fig. 4.

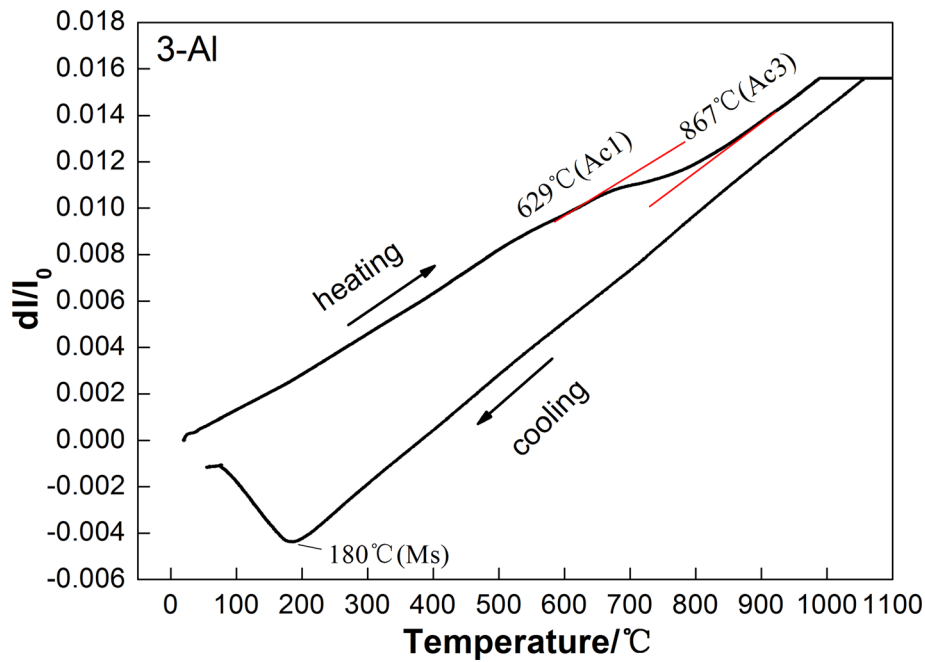


Fig. 2 Dilatometric curve showing intercritical temperature range

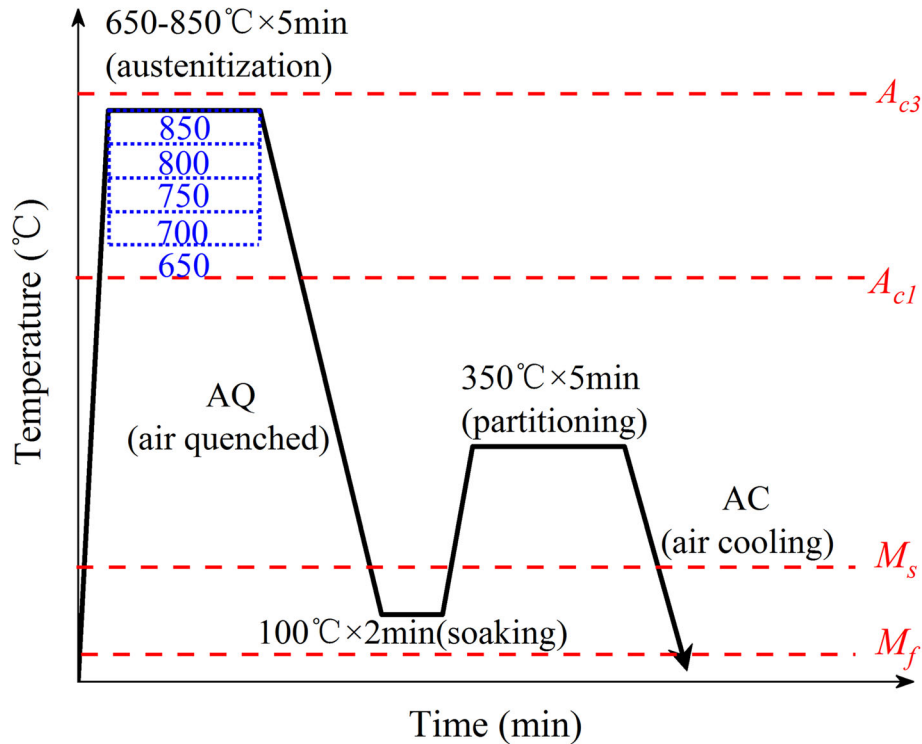


Fig. 3 Heat treatment process curve (Q and P) of experimental steel

3. Results

3.1 Mechanical Properties of Cold-Rolled Experimental Steel

Five tensile tests of experimental steels for each of two kinds of heat treatment processes were performed. The mechanical properties of experimental steels after Q and T process are

shown in Fig. 5. Figure 5(a) shows that with the increase in quenching temperature, the tensile strength of the steel increases gradually, and the total elongation of the steel reaches the peak ($52.5 \pm 2.1\%$) after quenching at 700 °C; at this time, the corresponding UTS is 1156 ± 14 MPa, and then, the total elongation of the steel begins to decrease. In addition, Fig. 5(b) shows that with the increase in quenching temperature, the PSE of the test steel first increases, and the PSE of the steel

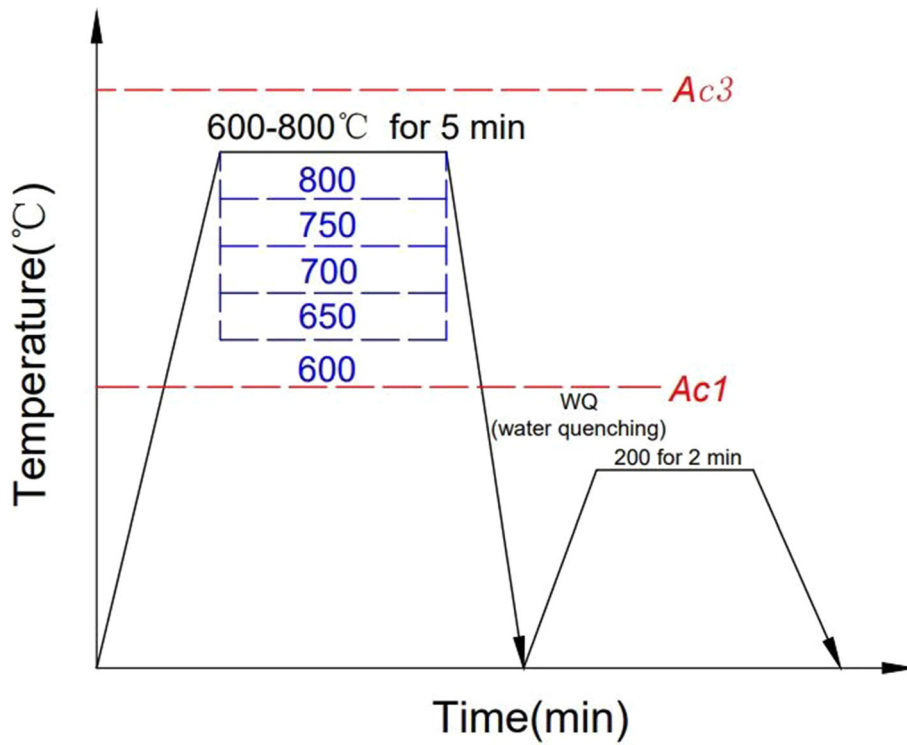


Fig. 4 Heat treatment process curve (Q and T) of experimental steel

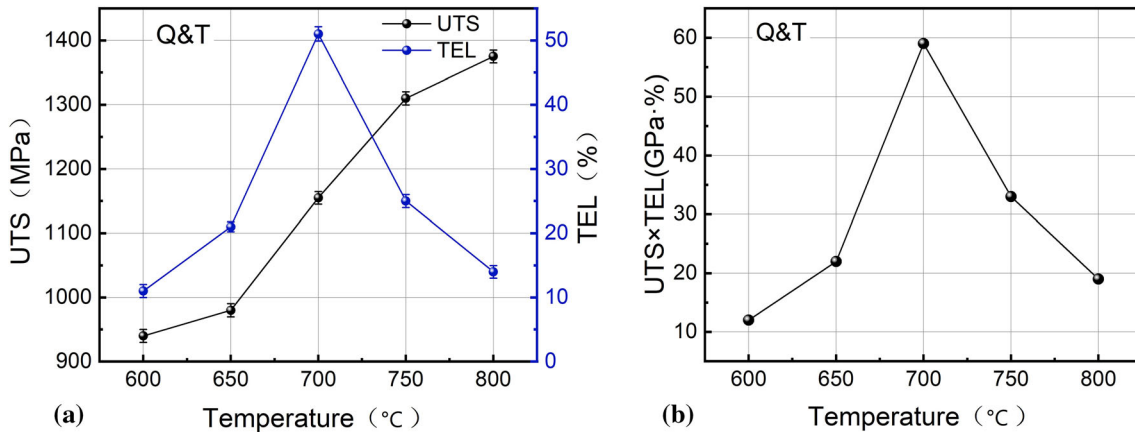


Fig. 5 Tensile properties curve of Q and T experimental steel. (a) UTS and TEL of experimental steel and (b) UTS \times TEL of experimental steel (UTS, ultimate tensile strength; TEL, total elongation)

quenched at 700 °C reaches the peak (59.5 GPa%), then the PSE decreases with the increase in quenching temperature, and the change in trend of the PSE is consistent with the change in trend of TEL of the experimental steels.

The mechanical properties of experimental steels treated with Q and P process are shown in Fig. 6. Figure 6(a) shows that with the increase in quenching temperature, the tensile strength of the steel will gradually decrease, but the degree of reduction is very small. The UTS of the steel quenched at 800 °C is the smallest, which is 890 ± 10 MPa. When the quenching temperature rises to 850 °C, the UTS of the steel increases greatly, reaching 1470 ± 24 MPa. The change trend of the total elongation of the steels is similar to that of the Q and T experimental steels, and the TEL of the Q and P experimental steel quenched at 750 °C is higher than that of the

Q and T experimental steel, the TEL of the Q and P experimental steel reaches the peak value ($47.4 \pm 1.7\%$), and the corresponding UTS is 908 ± 10 MPa. After that, the total elongation of the Q and P experimental steel begins to decrease. Figure 6(b) shows that with the increase in quenching temperature, the PSE of the experimental steel will first increase, when the quenching temperature reaches 750 °C, the PSE of the experimental steel reaches a peak value of 43 GPa%, and then, the PSE decreases with the increase in temperature.

3.2 Microstructure Evolution of Experimental Steel

Figure 7 shows the microstructure of experimental steels after Q and T treatment at different quenching temperatures. With increase in annealing temperature, the volume fraction

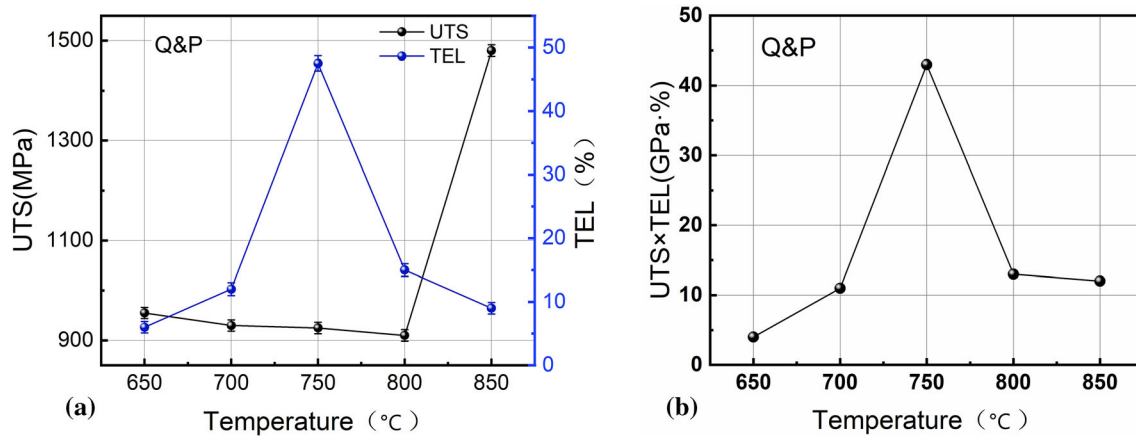


Fig. 6 Tensile properties curve of Q and P experimental steel. (a) UTS and TEL of experimental steel and (b) UTS × TEL of experimental steel

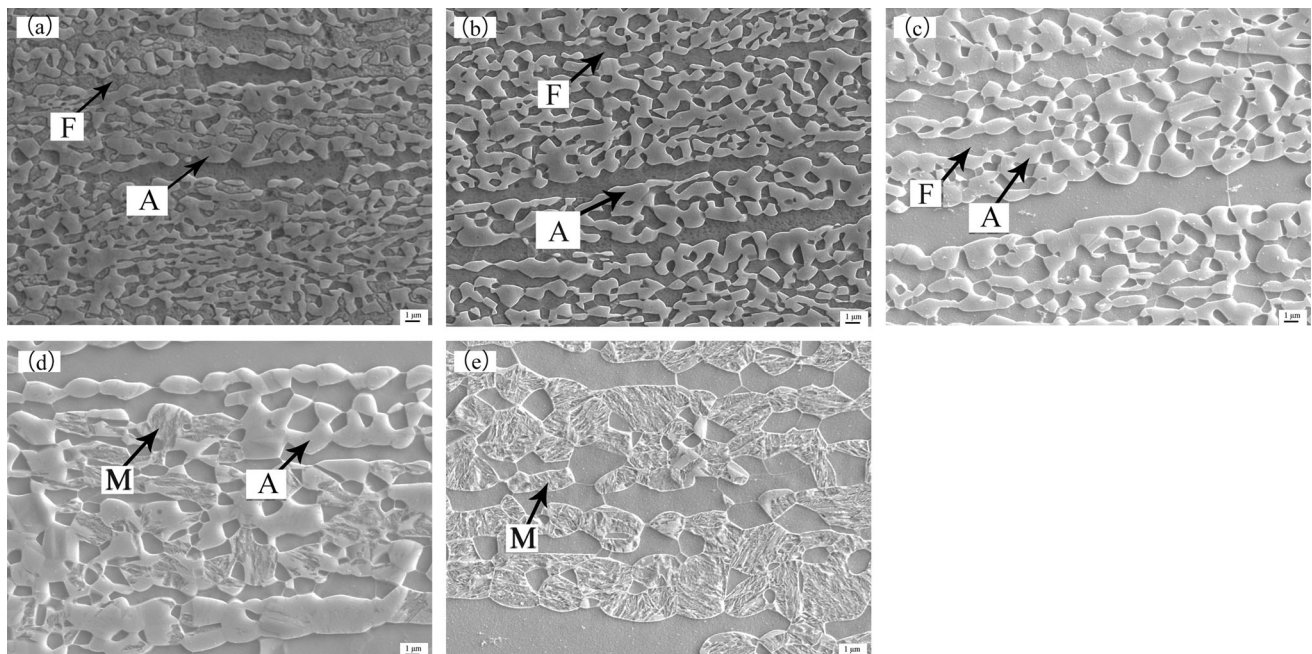


Fig. 7 SEM micrographs of Q and T cold-rolled samples after quenching from different temperatures (a—600 °C, b—650, c—700, d—750, e—800, A—Austenite, F—Ferrite, and M—Martensite)

and grain size of austenite is increased, and the volume fraction of ferrite is decreased during annealing in the intercritical region which is accord with the experimental results of steel annealing in 600-700 °C. The carbon and manganese content in austenite is higher than ferrite after annealing in the intercritical region. So, it is easy to define austenite and ferrite. The intercritical ferrite (IF) that formed during intercritical annealing has different morphologies with the layered δ -ferrite. For the steel annealing in 750-800 °C, austenite decreased distinctly owing to the extensive martensitic transformation and the transformed martensite got thicker and denser with elevated temperature.

Figure 7(a) shows that the main phases in the experimental steel quenched at 600 °C are austenite and ferrite, and ferrite is dominant. With the increase in quenching temperature, the content of austenite in the experimental steel increases gradually. When the quenching temperature was 700 °C, the

content of austenite phase reached the maximum (Fig. 7b and c), and when the quenching temperature was 750 °C, martensite began to appear in the experimental steel structure (Fig. 7d), so the volume fraction of austenite decreased accordingly. Figure 7(e) shows that when the quenching temperature was increased to 800 °C, more martensite appeared in the experimental steel, and the volume fraction of austenite decreased significantly. This change in trend was consistent with the XRD patterns of the experimental steels in Fig. 8. With the increase in quenching temperature, the integrated intensities of γ -FCC phase diffraction peaks ($(200)_\gamma$, $(311)_\gamma$ and $(220)_\gamma$) first increased and then decreased, the maximum value appeared at 700 °C. The volume fraction of austenite was calculated according to Eq. 1 (Ref 17, 18). Figure 9 shows the change in the volume fraction of austenite in the experimental steel for each quenching temperature during Q and T heat treatment. With the increase in quenching temperature, the

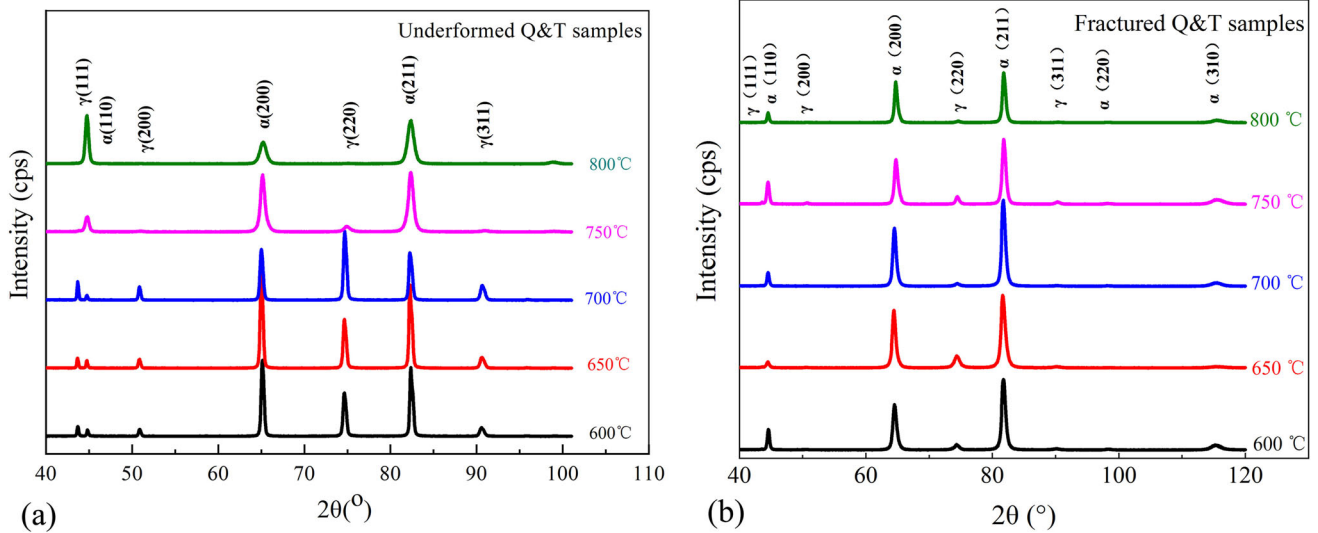


Fig. 8 XRD patterns for underformed and fractured Q and T steels

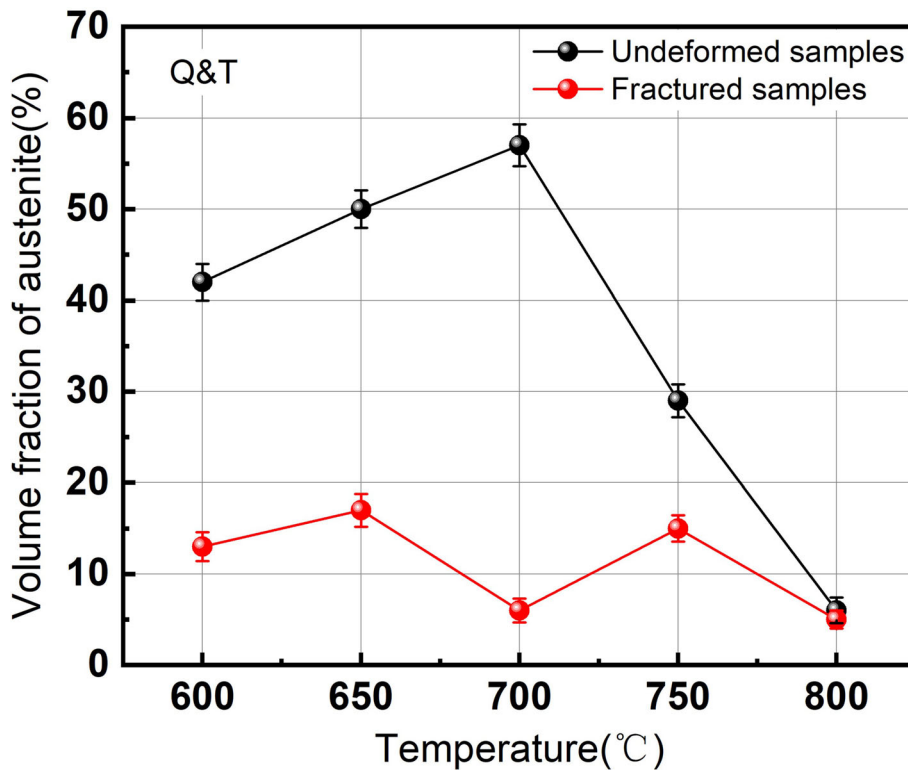


Fig. 9 Measured austenite volume fraction of Q and T experimental steel before and after tensile deformation at different temperatures

volume fraction of austenite in the experimental steel increased gradually. After quenching at 700 °C, the volume fraction of austenite reached the peak (59.5 vol.%). Then, with the increase in quenching temperature, the volume fraction of austenite in the experimental steel started to decrease. Measured austenite volume fraction of Q and T experimental steel after tensile deformation at different temperatures is presented in the red lines of Fig. 9.

Figure 10 shows the microstructural evolution in Q and P experimental steels at different quenching temperatures. Figure 10(a), (b), (c), (d), and (e) and 11 shows that the phase in

the Q and P experimental steel quenched at 650 °C is mainly ferrite, and a high content of austenite is not observed in Fig. 10(a), and the XRD pattern also showed that the diffraction peaks of γ -FCC phase of (200) $_{\gamma}$, (311) $_{\gamma}$, and (220) $_{\gamma}$ were not significant. When the quenching temperature was increased, a large number of austenite phase began to appear in the experimental steel. The proportion of austenite phase was further increased when the quenching temperature was 750 °C, and a small amount of martensite appeared in the microstructure of Q and P sample (Fig. 10c). When the quenching temperature was increased to 800 °C, the proportion of

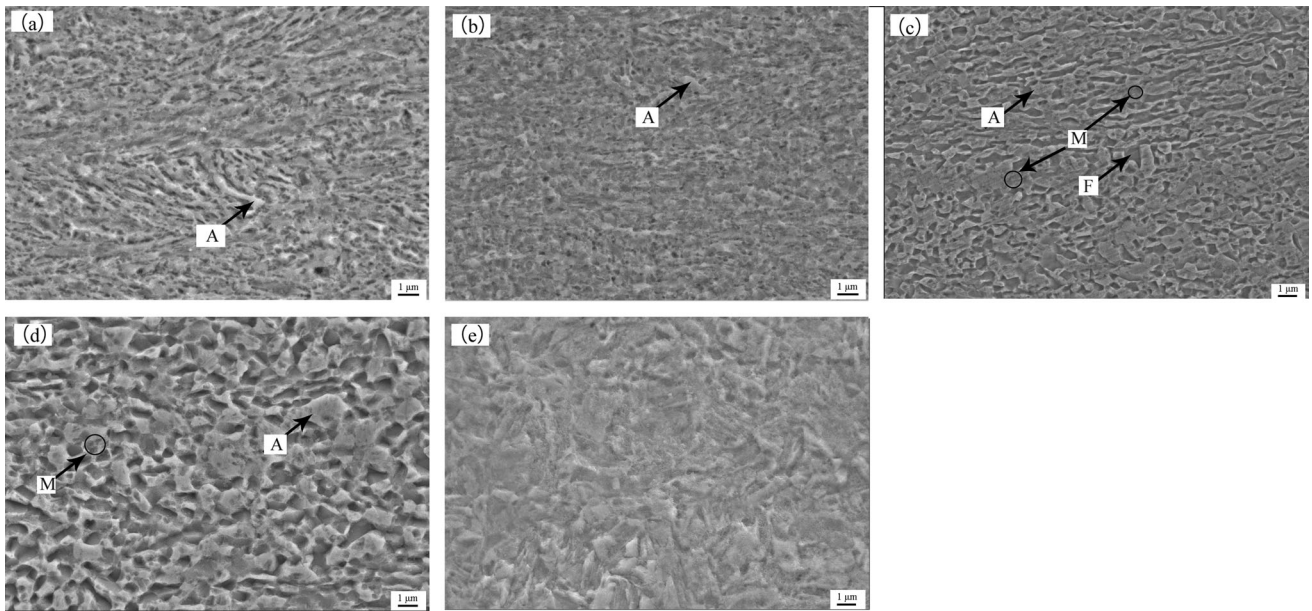


Fig. 10 SEM micrographs of Q and P cold-rolled samples after quenching from different temperatures (a—650 °C, b—700, c—750, d—800, and e—850)

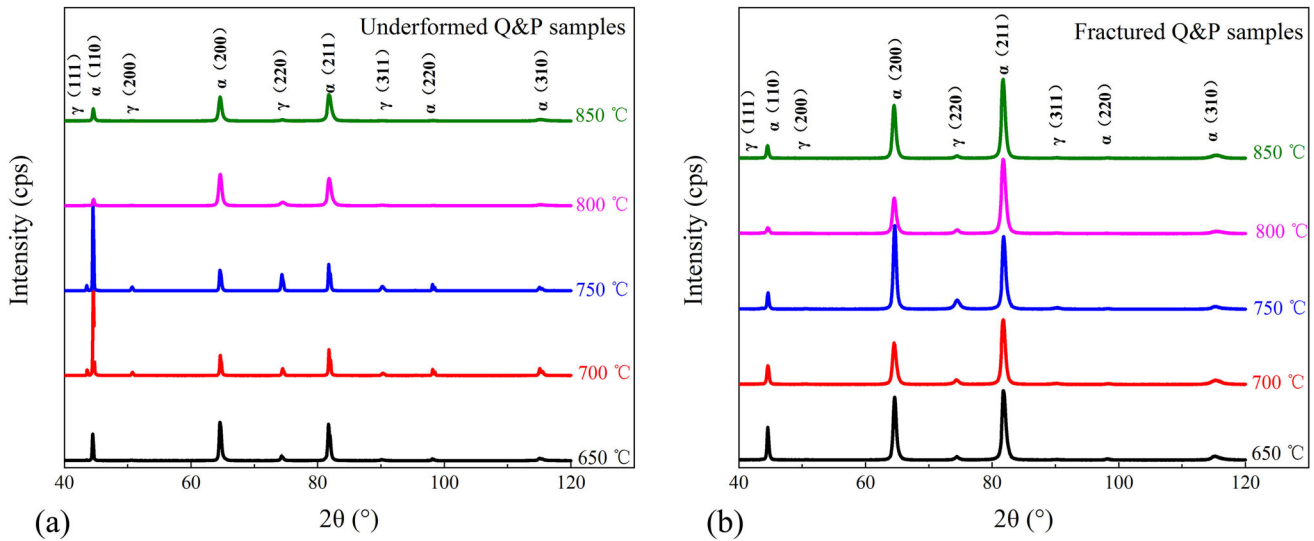


Fig. 11 XRD patterns for underformed and fractured Q and P steels

martensite increased, the volume fraction of austenite decreased, and the grains became coarser (Fig. 10d). The austenite content of Q and P sample further decreased when the quenching temperature was increased to 850 °C. The austenite volume fraction of Q and P samples at different quenching temperatures is also shown in Fig. 12. With the increase in quenching temperature, the volume fraction of austenite in the experimental steel increased gradually. After quenching at 750 °C, the volume fraction of austenite reached the peak (45 vol.%). Subsequently, with the increase in quenching temperature, the volume fraction of austenite in the experimental steel started to decrease. Measured austenite volume fraction of Q and P experimental steel after tensile deformation at different temperatures is presented in the red lines of Fig. 12.

3.3 Elemental Distribution in Austenite

Figure 13 shows a TEM micrograph of the undeformed experimental steel after two different heat treatments and the content of Mn at some marked points, and the points are marked across an austenite grain. Mn distribution in austenite is determined by energy-dispersive spectroscopy on the TEM. The distance between each measurement point is 0.3 μm. Figure 13(a) and (b) shows that the main phases in the structure of Q and P sample quenched at 750 °C (abbreviated as Q and P-750 sample) were austenite and ferrite. It may also be noted that the content of Mn in austenite was relatively high and evenly distributed, while the content of Mn in ferrite around austenite was relatively low. Figure 13(c) and (d) shows that the microstructure of Q and T sample quenched at 600 °C continued to be mainly composed of austenite and ferrite.

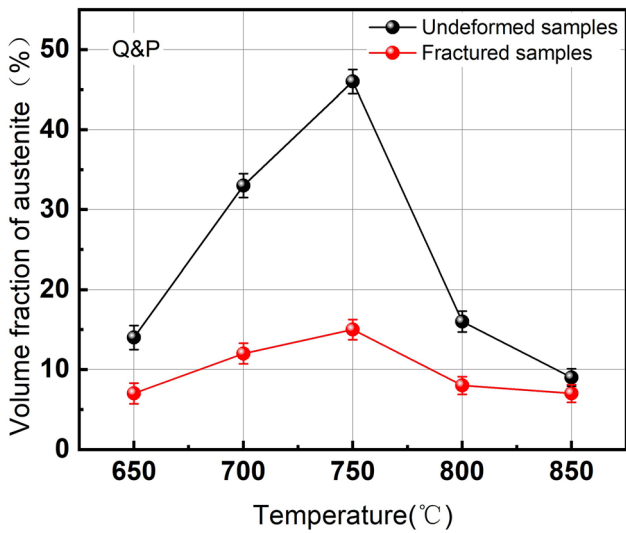


Fig. 12 Measured austenite volume fraction of Q and P experimental steel before and after tensile deformation at different temperatures

Compared with Q and P-750 sample, the volume fraction of austenite and ferrite in the two samples had little difference. In Q and T-600 sample, the content of Mn in ferrite was relatively low, and that in austenite was relatively high, but the distribution of Mn in austenite was uneven, the content of Mn in austenite boundary was relatively high, and that in austenite center was relatively low.

4. Discussion

4.1 Relationship Between Microstructure and Mechanical Properties of Q and T and Q and P Samples

In Q and P samples, when the quenching temperature was 650 °C, Fig. 6, 10(a), and 12 shows that the low volume fraction of austenite in the experimental steel resulted in weak TRIP effect, poor strength, and plasticity during deformation. When the quenching temperature rose to 700 °C, the austenite in the experimental steel was increased, such that the TRIP effect was slightly enhanced during the deformation process.

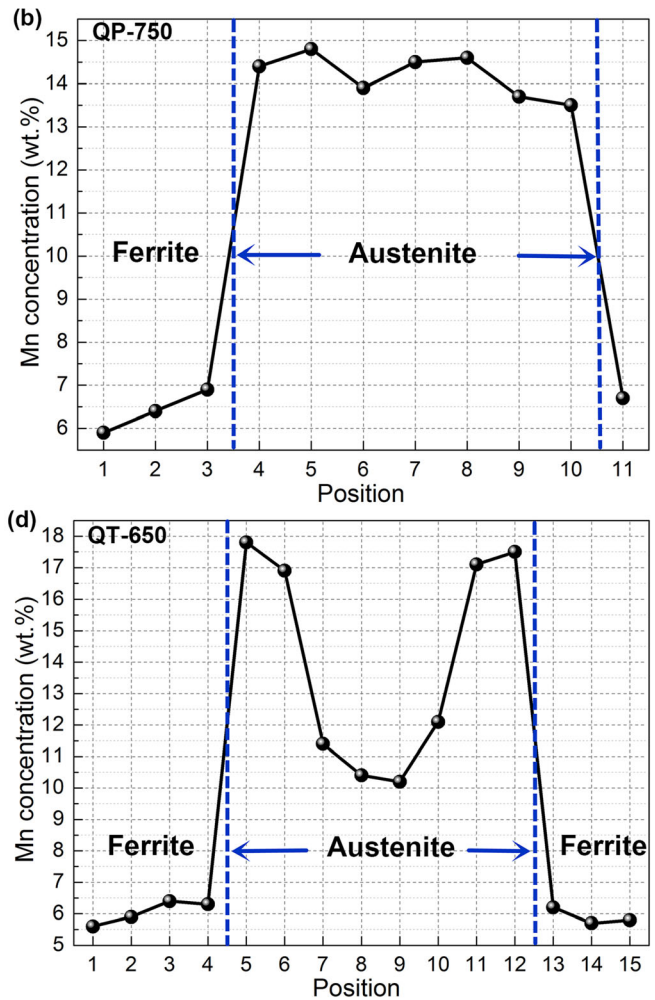
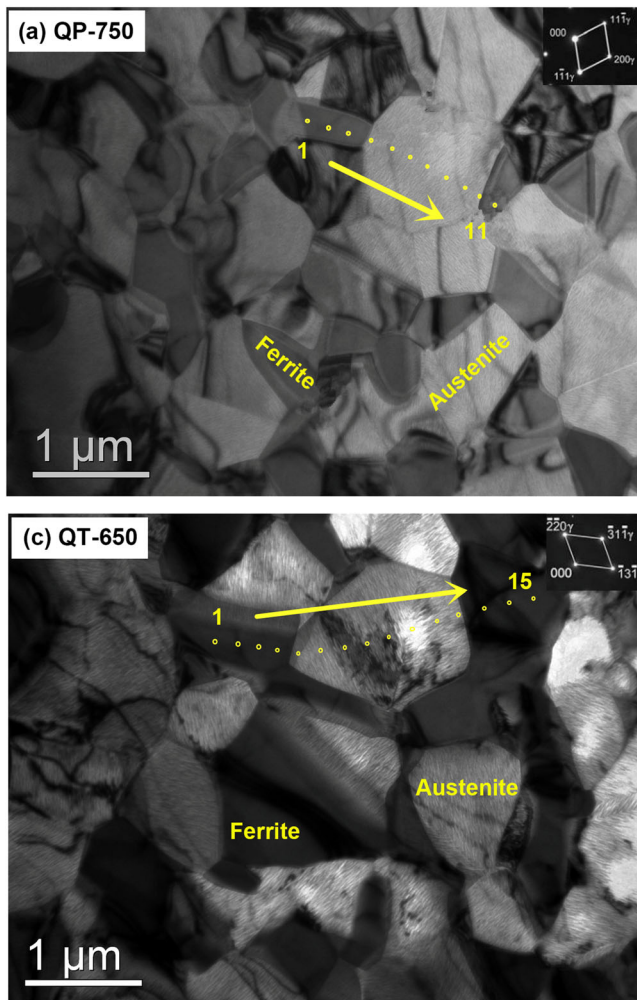


Fig. 13 TEM micrographs of Q and P-750 and Q and T-600 sample and Mn distribution in austenite are determined by energy-dispersive spectroscopy on the TEM. The distance between each measurement point is 0.3 μm

However, austenite has FCC structure, with more slip systems and easy to deform. Therefore, the plasticity of the experimental steel quenched at 700 °C was increased (Ref 19), but the strength was slightly decreased (Fig. 6). When the sample was quenched at 750 °C, the austenite content in the steel without deformation was increased (Fig. 12). With the increase in annealing temperatures, austenite grain size increases, but the stability of austenite decreases. During quenching, more austenite transforms into martensite. When the steel was annealed at 750 °C, only a small amount of austenite transformed into quenched martensite.

Austenite was still dominant in the steel after heat treatment (Fig. 10c), and the volume fraction of austenite reached 46.61% (Fig. 12), followed by ferrite, which is a soft phase, and can coordinate with austenite deformation during tensile straining. Moreover, TRIP effect occurred during austenite deformation, which promoted plastic deformation and improved the strength and ductility of Q and P steel. Figure 12 shows that the volume fraction of austenite of Q and P-750 sample decreased significantly after tensile fracture, which indicated that there was a strong TRIP effect during tensile straining of experimental steel, and the austenite transformation ratio reached 66.5%. Therefore, the Q and P sample quenched at 750 °C had the best total elongation and PSE (UTS: 908 ± 10 MPa, TEL: $47.4 \pm 1.7\%$, and PSE: 43 GPa%).

When the quenching temperature was 800 °C, martensite appeared in the steel (Fig. 10d), martensite is hard phase, and the volume fraction of austenite and ferrite was decreased because of the increase in the volume fraction of martensite (the volume fraction of austenite decreased to 15%), which was not conducive to softening effect of ferrite, but also reduced the TRIP effect of austenite. At the same time, the decrease in austenite content made it hard to absorb dislocations in martensite put forward by Pro Ma (Ref 20), grain boundary brittleness appeared, which reduced the TEL of the experimental steel. On the other hand, the morphology of Q and P sample quenched at 800 °C became coarse after quenching, which affected the strength and ductility, resulting in the decrease in UTS and TEL. A large amount of martensite was obtained in the Q and P sample quenched at 850 °C, which enhanced the tensile strength of the experimental steel (Fig. 6).

In the case of Q and T process (Fig. 5), both UTS and TEL increasing continuously with quench temperature increasing from 600 to 700 °C, which is attributed to the TRIP effect occurs during tensile deformation. Moreover, the volume fraction of austenite was increased gradually (Fig. 9), such that the TRIP effect enhanced gradually during deformation, and the PSE of Q and T sample was increased with the increase in quenching temperature. The volume fraction of austenite in Q and T-700 steel attained the highest value of 59.5% (Fig. 9), and the transformation ratio of austenite reached the highest value of 90.3% after tensile deformation, which indicated that strong TRIP effect occurred during the tensile process. Therefore, the PSE of the steel attained maximum value after quenching at 700 °C. As the quenching temperature increased to 750 °C, martensite began to appear in the Q and T sample, and the volume fraction of austenite decreased. When the quenching temperature increased from 750 to 800 °C, the volume fraction of martensite increased and the volume fraction of austenite decreased, which was responsible for the increase in UTS and decrease in TEL, respectively (Fig. 5, 7, and 9).

4.2 Effect of Heat Treatment Process on Distribution of C and Mn in Austenite

As shown in Fig. 13, the distribution of Mn in the microstructure of the samples treated by Q and P and Q and T is different. The distribution of Mn in austenite of Q and P-750 sample was relatively average, while that of Q and T-600 sample was enriched at the grain boundary regions of austenite, and the content of Mn in the center of austenite was relatively low. About 5-8 different visual fields for each sample were selected and repeated the TEM-EDS. The final conclusion obtained is the same. This is because the annealing time of Q and P process was longer, such that the elements had more time to diffuse, and Mn could completely diffuse to the core of austenite. In addition, in the partial austenitizing stage and subsequent quenching process of Q and P experimental steel, Mn in steel diffused from ferrite to austenite. On quenching of Q and P-750 steel, there was a small amount of martensite in the microstructure (Fig. 10c), and in the subsequent partitioning process, the ferrite and martensite in the steel experienced further transfer of C, and C further entered into austenite leading to uniformity in the distribution of C and Mn elements in austenite (Ref 21).

Q and T-600 sample had only one-step quenching process, and the steel recovered and recrystallized during the partial austenitizing condition, C and Mn alloying elements transferred and distributed in this stage. Q and T sample had only this one step of diffusion of alloying elements, and the diffusion time was too short. In this stage of recrystallization, there were only austenite and ferrite in the microstructure of Q and T sample, and ferrite was the only source of diffusion of carbon and manganese into austenite. Therefore, the diffusion of alloying elements was insufficient, carbon and manganese tend to segregate at the grain boundaries of austenite, resulting in higher content of C and Mn at the boundaries of austenite grains and lower content of C and Mn in the core of austenite grains. Austenite grain size is one of the reasons that affect the stability of austenite. However, the study found that the larger the austenite grain size, the lower the concentration of C/Mn elements in austenite. The smaller the austenite grain size, the higher the concentration of C/Mn elements. Therefore, the content of C/Mn elements in austenite is one of the important factors affecting its stability.

4.3 Factors Affecting Austenite Stability

There are many factors affecting the stability of austenite, such as C content, Mn content, austenite grain size, austenite morphology, and Schmidt factor. In this study, the content of C and Mn in austenite and the morphology of austenite had obvious influence on stability.

Compared with the Q and T steel, the austenite in the Q and P steel was more stable. In the Q and T heat treatment scheme, the austenite content of the experimental steel quenched at 600 and 650 °C was 43 and 51 vol.% (Fig. 9), which was similar to that of the Q and P experimental steel quenched at 750 °C (45 vol.%). Moreover, the austenite transformation ratio of Q and T-600, Q and T-650, and Q and P-750 samples after fracture was similar (Fig. 14). However, the TEL of Q and P-750 sample could reach $47.4 \pm 1.7\%$, which was much higher than that of Q and T-600 and Q and T-650 samples by $12.5 \pm 1.5\%$ and $22 \pm 1.4\%$ (Fig. 5 and 6). In addition, their tensile strength

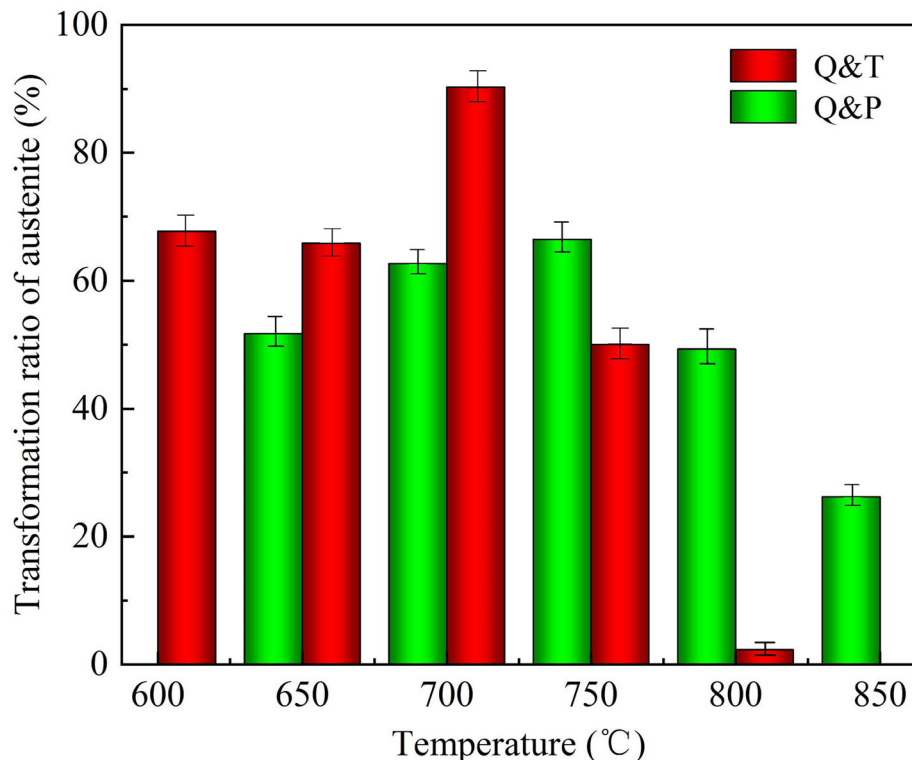


Fig. 14 Austenite transformation ratio of two heat treatment experimental steels

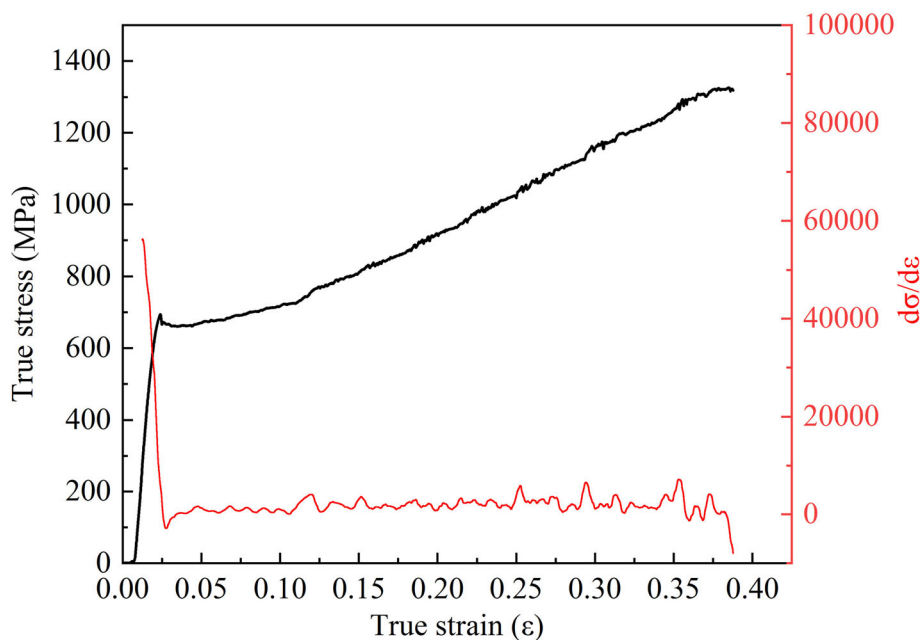


Fig. 15 True stress–strain curve and work hardening rate of Q and P experimental steel (quenched at 750 °C)

was similar (Q and T-600-942 ± 11 MPa, Q and T-650-982 ± 12 MPa, and Q and P-750-908 ± 10 MPa).

By comparing the true stress–strain and work hardening rate curves of Q and P-750 and Q and T-600 samples (Fig. 15 and 16), it can be seen that when the true strain of Q and P-750 sample reached ~ 2.5%, the decrease rate of work hardening rate curve slowed down, and the TRIP effect began to occur,

and the work hardening rate curve became stable, indicating that a continuous and stable TRIP effect has occurred.

However, when the strain of Q and T-600 sample was less than 1%, there was a short process of retardation of the decrease rate of work hardening rate curve, and then, the work hardening rate plateau appeared again when the strain was about 2.5%. The lower the stability of austenite, the smaller the strain will

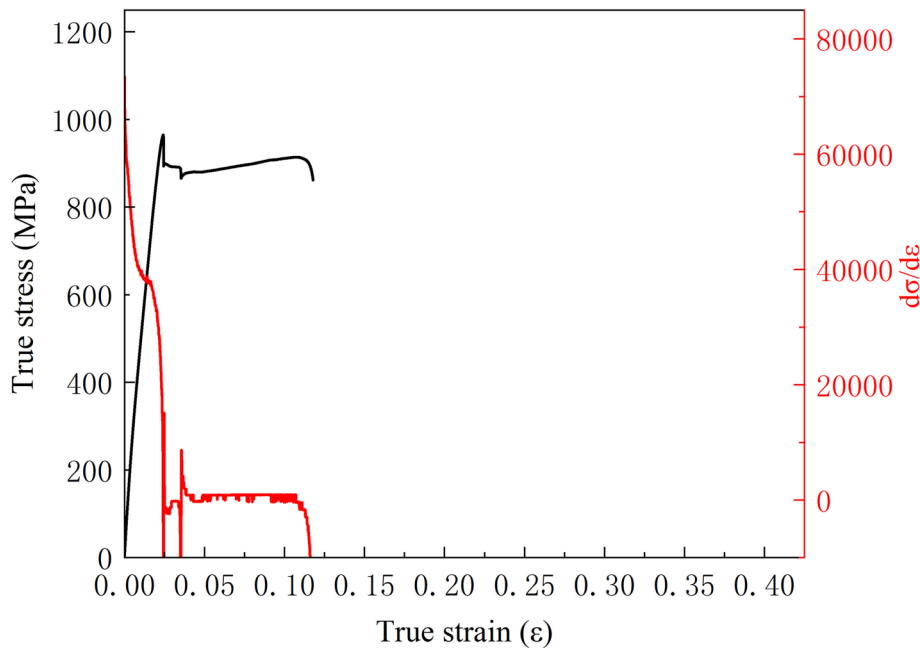


Fig. 16 True stress–strain curve and work hardening rate of Q and T experimental steel (quenched at 600 °C)

induce austenite to undergo phase transformation. And TRIP effect occurred at a small strain in Q and T-600 sample. It is implied that the austenite stability of Q and T-600 sample was low, and the TRIP effect appeared earlier in the early stage of deformation, but the subsequent TRIP effect could not continue to happen, which was unfavorable for elongation.

This was because the content of carbon and manganese in austenite of Q and T sample was less, and the distribution was uneven, C and Mn elements were distributed at the boundary of austenite, which reduced its stability (Ref 14, 22–25), while Q and P sample could enrich more C and Mn elements, and the distribution of alloy elements was more uniform, so it became more stable. In the case of tensile deformation, austenite with higher stability only undergoes phase transformation and induces TRIP effects at higher strains, which makes the TRIP effect last longer in TRIP steels with higher stability austenite.

Compared with Q and P sample, Q and T-700 sample had the best comprehensive mechanical properties (UTS—1156 ± 14 MPa, TEL—52.5 ± 2.1%, and PSE—59.5 GPa). This is because Q and T-700 sample had the highest volume fraction of austenite (59.5 vol.%) before tensile test, which could be seen from Fig. 9. Therefore, Q and T-700 sample was more likely to experience a strong TRIP effect during tensile straining. In addition, Fig. 9 also shows that the Q and T-700 sample had obvious TRIP effect during tensile deformation, and the austenite transformation ratio was as high as 90.3% (Fig. 14).

During the partitioning process of Q and P-850 experimental steel, the microstructure included austenite, ferrite, and martensite, and there were more carbon atom diffusion paths (Ref 26–28), so the austenite contained more carbon atom. However, because of the coarse grains caused by too high quenching temperature, the stability of austenite was poor (Ref 29). It can be seen that the strain hardening rate decreased rapidly at the beginning of deformation from curves of true stress–strain and work hardening rate (as shown in Fig. 17), which is attributed to the deformation of ferrite. When the true strain reached 1%, the decrease in the rate of work hardening rate slowed down,

which was caused by TRIP effect. The TRIP effect of Q and P-850 sample occurred earlier compared to Q and P-750 sample, which decreased the rate of the work hardening rate when the true strain reached 2.5%. At the same time, due to the high content of hard phase martensite and large morphology in Q and P-850 experimental steel, which led to early fracture of the sample. Austenite–martensite transformation of Q and P-850 sample did not occur completely out during deformation (austenite transformation ratio was only 26.2%), which led to weak TRIP effect in the experimental steel and reduced the TEL of the experimental steel. Figure 15 and 17 shows that there was a long plateau of work hardening rate in the work hardening rate curve of Q and P-750 experimental steel, which corresponded to a stronger and more durable TRIP effect in the experimental steel, while the TRIP effect of Q and P-850 experimental steel was weaker, and its work hardening rate plateau was shorter.

Austenite should have an appropriate stability range. Too high or too low austenite stability is not conducive to the TRIP effect and is not conducive to improving its work hardening ability. The TRIP effect has a dual effect on the mechanical properties of medium manganese steel, that is, the occurrence of the TRIP effect under small strain conditions not only cannot improve the work hardening ability and mechanical properties, but also reduces the plasticity of the material due to the premature occurrence of the TRIP effect. However, if the TRIP effect occurs only at large strains, it is not necessary to improve the work hardening ability and mechanical properties of the material.

The above results and discussion confirmed that that high C content, Mn content, and fine grain size in austenite can improve the stability of austenite. But for the TRIP effect and mechanical properties of steel, it is not true that higher the stability of austenite, the more superior is the TRIP effect. If the austenite is too stable, the TRIP effect is induced when the degree of deformation is preferably large. At this time, there is a large accumulation of stress, and some microcracking may

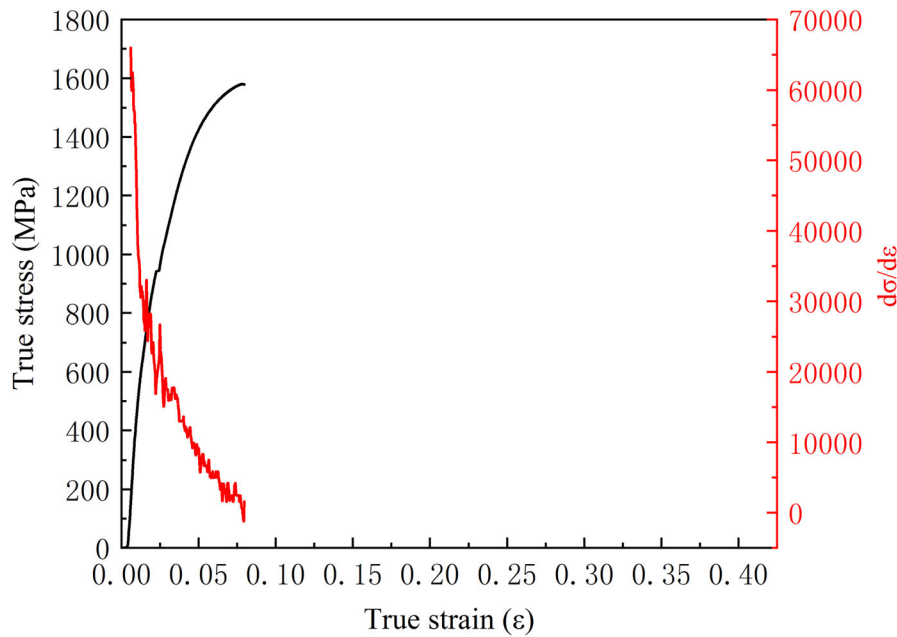


Fig. 17 True stress–strain curve and work hardening rate of Q and P experimental steel (quenched at 850 °C)

occur, which may lead to the early fracture of the steel. Therefore, in order to improve the mechanical properties of steel through TRIP effect, the austenite in the steel should have appropriate stability, neither too high nor too low. Compared with Q and P heat treatment process, the PSE of 0.2C-8.5Mn-3Al-Fe cold-rolled experimental steel after Q and T heat treatment was higher, and the process is simpler.

5. Conclusions

- (1) By comparing the mechanical properties and austenite content of the experimental steels treated by Q and T and Q and P process, it is found that the tensile strength of the experimental steels treated by Q and T and Q and P is similar, but the specimens treated by Q and P can attain higher TEL. The TRIP effect has a dual effect on the mechanical properties of medium manganese steel, TRIP effect under small strain conditions not only cannot improve the work hardening ability and mechanical properties, but also reduces the plasticity of the material.
- (2) Given that the heat treatment time of Q and T sample is relatively short, the diffusion of Mn is relatively insufficient, the distribution of Mn in austenite is uneven, the content of Mn at the edge of austenite is greater, and the content of Mn in the center is less, which led to low stability of austenite. If austenite–martensite transformation occurs in a short time during the early stage of deformation, then elongation by TRIP effect is less.
- (3) When the diffusion time of alloying elements in Q and P samples is relatively long, Mn can diffuse, and the distribution of Mn element in austenite is relatively uniform, such that the stability of austenite in samples is high. Austenite with relatively high stability can delay

TRIP effect during deformation, which provides strong work hardening ability and improves TEL.

- (4) Compared with the experimental steel with only ferrite and austenite, austenite of experimental steel with ferrite, austenite, and martensite in the microstructure has different ways to obtain carbon. The larger the austenite grain size, the lower the concentration of C/Mn elements in austenite. The smaller the austenite grain size, the higher the concentration of C/Mn elements. It is suggested that there may be different mechanisms of carbon diffusion between ferrite–austenite and martensite–austenite.

Acknowledgments

This research was funded by the National Natural Science Foundation of China, Grant No. 52005304, Science and Technology Plan for Youth Innovation Team in Colleges and Universities of Shandong Province (2022KJ219), National Natural Science Foundation of China (52175342), and The Natural Science Foundation of Shandong (ZR2021ME129). The authors are grateful to R.D.K. Misra for continued collaboration and contribution to meaningful discussion.

Data Availability

The raw/processed data required to reproduce these findings cannot be shared at this time as the data also form part of an ongoing study.

Conflict of interest

The authors declare that they have no conflict of interest.

References

1. S. Lee, S.J. Lee, and B.C. De Cooman, Austenite Stability of Ultrafine-Grained Transformation-Induced Plasticity Steel with Mn Partitioning, *Scr. Mater.*, 2011, **65**(3), p 225–228.
2. D.W. Suh and S.J. Kim, Medium Mn Transformation-Induced Plasticity Steels: Recent Progress and Challenges, *Scr. Mater.*, 2017, **126**, p 63–67.
3. Z.C. Li, H. Ding, R.D.K. Misra, and Z.H. Cai, Deformation Behavior in cold-Rolled Medium-Manganese TRIP Steel and Effect of Pre-strain on the Lüders Bands, *Mater. Sci. Eng. A*, 2017, **679**, p 230–239.
4. Z.C. Li, X.T. Zhang, Y.J. Mou, Z.H. Cai, R.D.K. Misra, L.F. He, H.P. Li, and H. Ding, Design of an Effective Heat Treatment Involving Intercritical Hardening for High-Strength–High Elongation of 0.2C–1.5Al-(6–8.5)Mn-Fe TRIP Steels: Microstructural Evolution and Deformation Behaviour, *Mater. Sci. Technol.*, 2020, **36**(4), p 500–510.
5. G.-J. Cheng, B. Gault, C.-Y. Huang, C.-Y. Huang, and H.-W. Yen, Warm Ductility Enhanced by Austenite Reversion in Ultrafine-Grained Duplex Steel, *Acta Mater.*, 2018, **148**, p 344–354.
6. J. Speer, D.K. Matlock, B.C. De Cooman, and J.G. Schroth, Carbon Partitioning into Austenite After Martensite Transformation, *Acta Mater.*, 2003, **51**(9), p 2611–2622.
7. S.J. Kim, G.L. Chang, T.H. Lee, and C.S. Oh, Effect of Cu, Cr and Ni on Mechanical Properties of 0.15 wt.% C TRIP-Aided Cold Rolled Steels, *Scr. Mater.*, 2003, **48**(5), p 539–544.
8. H. Luo, H. Dong, and M. Huang, Effect of Intercritical Annealing on the Lüders Strains of Medium Mn Transformation-Induced Plasticity Steels, *Mater. Design*, 2015, **83**, p 42–48.
9. P.J. Gibbs, E. De Moor, M.J. Merwin, B. Clausen, J.G. Speer, and D.K. Matlock, Austenite Stability Effects on Tensile Behavior of Manganese-Enriched-Austenite Transformation- Induced Plasticity Steel, *Metall. Mater. Trans. A*, 2011, **42**(12), p 3691–3702.
10. H. Pan, M. Cai, H. Ding, S. Sun, H. Huang, and Y. Zhang, Ultrahigh Strength-Ductile Medium-Mn Steel Auto-Parts Combining Warm Stamping and Quenching & Partitioning, *Mater. Sci. Technol.*, 2019, **35**(7), p 807–814.
11. B. Hu, H. Luo, F. Yang, and H. Dong, Recent Progress in Medium-Mn Steels Made with New Designing Strategies, *J. Mater. Sci. Technol.*, 2017, **33**(12), p 1457–1464.
12. Z.C. Li, R.D.K. Misra, Z.H. Cai, H.X. Li, and H. Ding, Mechanical Properties and Deformation Behavior in Hot-Rolled 0.2C–1.5/3Al-8.5Mn-Fe TRIP Steel: The Discontinuous TRIP Effect, *Mater. Sci. Eng. A*, 2016, **673**, p 63–72.
13. Z.C. Li, H. Ding, R.D.K. Misra, and Z.H. Cai, Microstructure-Mechanical Property Relationship and Austenite Stability in Medium-Mn TRIP Steels: The Effect of Austenite-Reverted Transformation and Quenching-Tempering Treatments, *Mater. Sci. Eng. A*, 2017, **682**, p 211–219.
14. Y. Li, W. Li, N. Min, W. Liu, and X. Jin, Effects of Hot/Cold Deformation on the Microstructures and Mechanical Properties of Ultra-Low Carbon Medium Manganese Quenching-Partitioning-Tempering Steels, *Acta Mater.*, 2017, **139**, p 96–108.
15. A.K. Srivastava, D. Bhattacharjee, G. Jha, N. Gope, and S.B. Singh, Microstructural and Mechanical Characterization of C-Mn-Al-Si Cold-Rolled TRIP-Aided Steel, *Mater. Sci. Eng. A*, 2007, **445–446**, p 549–557.
16. E. De Moor, D.K. Matlock, J.G. Speer, and M.J. Merwin, Austenite Stabilization Through Manganese Enrichment, *Scr. Mater.*, 2011, **64**(2), p 185–188.
17. N. Vandijk, A. Butt, L. Zhao, J. Sietsma, S. Offerman, J. Wright, and S. Vanderzwaag, Thermal Stability of Retained Austenite in TRIP Steels Studied by Synchrotron X-ray Diffraction During Cooling, *Acta Mater.*, 2005, **53**(20), p 5439–5447.
18. M.C. Jo, J. Park, S.S. Sohn, S. Kim, J. Oh, and S. Lee, Effects of Untransformed Ferrite on Charpy Impact Toughness in 1.8-GPa-Grade Hot-Press-Forming Steel Sheets, *Mater. Sci. Eng. A*, 2017, **707**, p 65–72.
19. B. Hu and H. Luo, A Novel Two-Step Intercritical Annealing Process to Improve Mechanical Properties of Medium Mn Steel, *Acta Mater.*, 2019, **176**, p 250–263.
20. Z.H. Cai, D.L. Zhang, L.F. Ma, H. Ding, Y. Feng, J. Hu, and R.D.K. Misra, Competing Deformation Mechanisms in an Austenite-Ferrite Medium-Mn Steel at Different Strain Rates, *Mater. Sci. Eng. A*, 2021, **818**, p 141357.
21. H.L. Cai, P. Chen, J.K. Oh, Y.R. Cho, D. Wu, and H.L. Yi, Quenching and Flash- Partitioning Enables Austenite Stabilization During Press-Hardening Processing, *Scr. Mater.*, 2020, **178**, p 77–81.
22. L. Liu, Q. Yu, Z. Wang, J. Ell, M.X. Huang, and R.O. Ritchie, Making Ultrastrong Steel Tough by Grain-Boundary Delamination, *Science*, 2020, **368**, p 1347–1358.
23. H. Pan, H. Ding, and M. Cai, Microstructural Evolution and Precipitation Behavior of the Warm-Rolled Medium Mn Steels Containing Nb or Nb-Mo During Intercritical Annealing, *Mater. Sci. Eng. A*, 2018, **736**, p 375–382.
24. G.J. Cheng, B. Gault, C.Y. Huang, C.Y. Huang, and H.W. Yen, Warm Ductility Enhanced by Austenite Reversion in Ultrafine-Grained Duplex Steel, *Acta Mater.*, 2018, **148**, p 344–354.
25. H.L. Cai, P. Chen, J.K. Oh, Y.R. Cho, D. Wu, and H.L. Yi, Quenching and Flash-Partitioning Enables Austenite Stabilization During Press-Hardening Processing, *Scr. Mater.*, 2020, **178**, p 77–81.
26. J. Zhang, H. Ding, and R.D.K. Misra, Enhanced Strain Hardening and Microstructural Characterization in a Low Carbon Quenching and Partitioning Steel with Partial Austenization, *Mater. Sci. Eng. A*, 2015, **636**, p 53–59.
27. C. Wang, H. Ding, M.H. Cai, and B. Rolfe, Characterization of Microstructures and tensile Properties of TRIP-Aided Steels with Different Matrix Microstructure, *Mater. Sci. Eng. A*, 2014, **610**, p 65–75.
28. C. Wang, H. Ding, M.H. Cai, and B. Rolfe, Multi-Phase Microstructure Design of a Novel High Strength TRIP Steel Through Experimental Methodology, *Mater. Sci. Eng. A*, 2014, **610**, p 436–444.
29. Z.H. Cai, D.L. Zhang, G.Q. Wen, L.F. Ma, and R.D.K. Misra, The Influence of Cooling Rate on Austenite Stability and Mechanical Properties in an Austenite-Ferrite Medium-Mn Steel, *J. Mater. Eng. Perform.*, 2021, **134**, p 7917–7925.

Publisher's Note Springer Nature remains neutral with regard to jurisdictional claims in published maps and institutional affiliations.

Springer Nature or its licensor (e.g. a society or other partner) holds exclusive rights to this article under a publishing agreement with the author(s) or other rightsholder(s); author self-archiving of the accepted manuscript version of this article is solely governed by the terms of such publishing agreement and applicable law.